Pergamon

Int. J. Solids Structures Vol. 35, Nos 34–35, pp. 4779–4801, 1998

Printed in Great Britain
0020-7683/98/$—see front matter

PII: S0020-7683(98)00094-8

TRANSMISSION LOSS IN A SHALLOW OCEAN OVER A TWO-LAYER SEABED

JAMES L. BUCHANAN†
Mathematics Department, United States Naval Academy, Annapolis MD 21402, U.S.A.

and

ROBERT P. GILBERT
Department of Mathematical Sciences, University of Delaware, Newark DE 19716, U.S.A.

(*Received* 10 *June* 1997; *in revised form* 25 *February* 1998)

Abstract—Three mathematical models of a two-layer seabed are considered. The first assumes that both layers are elastic solids, the second that the upper layer is poroelastic while the substrate is elastic, and the third that both layers are poroelastic. The first and third models are found to produce reasonable agreement with data and each other, but the second model produces poor predictions because of mathematical incompatibilities of the poroelastic and elastic models. © 1998 Elsevier Science Ltd. All rights reserved.

1. INTRODUCTION

In a shallow ocean sound waves travelling distances of several kilometers will interact with the underlying seabed repeatedly. Consequently in developing a mathematical means for predicting acoustic pressure in a shallow ocean the manner in which the seabed is modelled is important. In such computations the seabed typically is treated as a dense fluid, an elastic solid, or a poroelastic medium. As indicated in Vidmar (1980a, b) the fluid model is appropriate for thick sediment layers, but thin sediment layers, where conversion of energy to shear waves is an important loss mechanism, require a model which supports shear effects. Examples of the poor predictions made by the fluid model for thin sediment layers can be found in Hughes *et al.* (1990). Since thin surficial sediment layers are common in shallow ocean environments, we restrict consideration to the solid elastic and poroelastic models.

When the seabed is regarded as porous, the model developed by Biot (1956a, b, 1962) for a poroelastic medium is often used. The Biot model treats the medium as an elastic frame with interstitial pore fluid. Stoll (1974) modified the Biot model so that it depends upon more easily estimated parameters and introduced complex frame moduli to account for losses due to frame inelasticity. Unlike the elastic solid model, the Biot–Stoll model predicts a non-linear dependence on frequency for sediment attenuation. This is due to the presence of both viscous resistance to pore fluid motion which is the dominant source of loss at low frequencies, and frame inelasticity loss which predominates at higher frequencies (Stoll, 1977). This nonlinear dependence is most pronounced in coarse, high permeability sediments. The poroelastic model also predicts the existence of Type I and Type II compressional waves, the former correspond in speed and attenuation to the compressional wave in the elastic model, while the latter move more slowly and are highly attenuated in range. As indicated in Stoll (1977) conversion of Type I waves to Type II, as well as shear waves, at an interface represents a source of energy loss. Discussion and illustrations of these frequency dependencies for various sediments and the influence of individual parameters in the Biot model can be found in Yamamoto (1983a, b), as well as the works by Stoll which are cited above. Comparison of predictions made by the Biot–Stoll model with laboratory

† Supported in part by a U.S. Naval Academy Recognition Grant. Author to whom correspondence should be addressed. E-mail: jlb@sma.usna.navy.mil

and field measurements can be found in Brunson and Johnson (1980), Beebe *et al.* (1982) and Holland and Brunson (1988).

The differential equations of the Biot model are considerably more complicated than those of the elastic model. The works of Biot and Stoll cited above rely on one-dimensional solutions while Yamamoto (1983a) derives a modal solution in two Cartesian coordinates for the case of an ocean over a halfspace poroelastic seabed. When multiple sediment layers are present solution of the full set of equations with realistic interface conditions is algebraically formidable. In the multi-layer model of Ingenito *et al.* (1978) used for the predictions in Beebe *et al.* (1982) shear effects were not taken into account. With the assistance of computer algebra systems, however, solution of the full Biot model is now possible in the case of constant parameters. Results based upon this solution for the case of a one-layer seabed are presented in Buchanan and Gilbert (1997) and results for a poroelastic sediment over a rigid substrate in Buchanan and Gilbert (1996). In Buchanan and Gilbert (1998) transmission loss as computed from the analytic solution is shown to be in good agreement with loss computed using parabolic approximation. Computation of pressure in the near field is discussed in Buchanan *et al.* (1997) and again the results agree with those obtained by parabolic approximation at ranges where both approaches are expected to be valid.

In this article we compare predictions for transmission loss for a time-harmonic point source over a two-layer seabed for three different models: an elastic sediment over an elastic substrate, a poroelastic sediment over an elastic substrate, and a poroelastic sediment over a poroelastic substrate. Since the effects of sediment porosity are expected to be most significant in the surficial layer, and since for the substrate it is difficult to estimate even the five parameters of the elastic model, much less the thirteen of the Biot–Stoll model, the second of the three models is most appealing. It is one of the purposes of this work, however, to show that this model is mathematically flawed due to incompatibilities in the behavior of the eigenvalues between the elastic and poroelastic models.

2. THE POROELASTIC AND ELASTIC MODELS FOR A SEABED

In this section we set forth the differential equations for the poroelastic model developed in Biot (1956a, b), as well as those of the elastic model. Also presented are sets of Biot–Stoll parameters taken from the literature which will be used in the numerical results of subsequent sections.

2.1. *The Biot model for a poroelastic seabed*

The Biot model treats the medium as an elastic frame with interstitial pore fluid. Two displacement vectors $\mathbf{u}(x, y, z, t)$ and $\mathbf{U}(x, y, z, t)$ track the motions of the frame and fluid, respectively, while the divergences $e = \nabla \cdot \mathbf{u}$ and $\varepsilon = \nabla \cdot \mathbf{U}$ give the frame and fluid dilatations. The following constitutive relations are assumed

$$\begin{aligned}
\sigma_{xx} &= 2\mu e_{xx} + \lambda e + Q\varepsilon, \\
\sigma_{yy} &= 2\mu e_{yy} + \lambda e + Q\varepsilon, \\
\sigma_{zz} &= 2\mu e_{zz} + \lambda e + Q\varepsilon, \\
\sigma_{xy} &= \mu e_{xy}, \quad \sigma_{xz} = \mu e_{xz}, \quad \sigma_{yz} = \mu e_{yz}, \\
\sigma &= Qe + R\varepsilon. \qquad (1)
\end{aligned}$$

The parameters λ and μ are the Lamé coefficients of the elastic frame, R measures the pressure on the fluid required to force a certain volume of fluid into the sediment at constant volume, and Q measures the coupling of changes in the volume of the solid and fluid. As usual the strains are related to the displacements by

$$e_{xx} = \frac{\partial u_x}{\partial x}, \quad e_{xy} = \frac{\partial u_x}{\partial y} + \frac{\partial u_y}{\partial x}, \ldots. \tag{2}$$

Equations (1) and (2) and an argument based upon Lagrangian dynamics are shown in Biot (1956a) to lead to the following equations of motion for the displacements and dilatations

$$\begin{aligned} \mu\nabla^2\mathbf{u} + \nabla[(\lambda+\mu)e + Q\varepsilon] &= \frac{\partial^2}{\partial t^2}(\rho_{11}\mathbf{u} + \rho_{12}\mathbf{U}) + b\frac{\partial}{\partial t}(\mathbf{u}-\mathbf{U}) \\ \nabla[Qe + R\varepsilon] &= \frac{\partial^2}{\partial t^2}(\rho_{12}\mathbf{u} + \rho_{22}\mathbf{U}) - b\frac{\partial}{\partial t}(\mathbf{u}-\mathbf{U}) \end{aligned} \tag{3}$$

where ρ_{11} and ρ_{22} are density parameters for the solid and fluid, ρ_{12} is a density coupling parameter, and b is a dissipation parameter. All parameters are assumed to be constant in each sediment layer.

The seabed is assumed to oscillate harmonically in time: $\mathbf{u}(x, y, z, t) = \mathbf{u}(x, y, z)\, e^{i\omega t}$, $\mathbf{U}(x, y, z, t) = \mathbf{U}(x, y, z)\, e^{i\omega t}$. Substituting these representations into (3) gives

$$\begin{aligned} \mu\nabla^2\mathbf{u} + \nabla[(\lambda+\mu)e + Q\varepsilon] + p_{11}\mathbf{u} + p_{12}\mathbf{U} &= 0 \\ \nabla[Qe + R\varepsilon] + p_{12}\mathbf{u} + p_{22}\mathbf{U} &= 0 \end{aligned} \tag{4}$$

where

$$p_{11} := \omega^2\rho_{11} - i\omega b, \quad p_{12} := \omega^2\rho_{12} + i\omega b, \quad p_{22} := \omega^2\rho_{22} - i\omega b. \tag{5}$$

Taking the divergence and curl of both equations in (4) yields the system

$$\begin{aligned} \nabla^2((\lambda+2\mu)e + Q\varepsilon) + p_{11}e + p_{12}\varepsilon &= 0 \\ \nabla^2(Qe + R\varepsilon) + p_{12}e + p_{22}\varepsilon &= 0 \\ \mu\nabla^2\varpi + p_{11}\varpi + p_{12}\boldsymbol{\Omega} &= 0 \\ p_{12}\varpi + p_{22}\boldsymbol{\Omega} &= 0 \end{aligned} \tag{6}$$

where $\varpi := \times\mathbf{u}$ and $\boldsymbol{\Omega} := \nabla\times\mathbf{U}$.

In the first two equations of (6) we make the change of dependent variables

$$\tau := (\lambda+2\mu)e + Q\varepsilon, \quad \sigma := Qe + R\varepsilon, \tag{7}$$

the inverse transformation for which is

$$e = a_{11}\tau - a_{12}\sigma, \quad \varepsilon = -a_{12}\tau + a_{22}\sigma \tag{8}$$

where

$$a_{11} := R/d, \quad a_{12} := Q/d, \quad a_{22} := (\lambda+2\mu)/d$$

with

$$d := R(\lambda+2\mu) - Q^2.$$

This gives

$$\nabla^2\tau + B_{11}\tau + B_{12}\sigma = 0$$
$$\nabla^2\sigma + B_{21}\tau + B_{22}\sigma = 0 \tag{9}$$

where

$$B_{11} := a_{11}p_{11} - a_{12}p_{12}, \quad B_{12} := -a_{12}p_{11} + a_{22}p_{12},$$
$$B_{21} := a_{11}p_{12} - a_{12}p_{22}, \quad B_{22} := -a_{12}p_{12} + a_{22}p_{22}.$$

Once solutions to (9) are known, then upon substituting the representation for the fluid displacement vector

$$\mathbf{U} = -\frac{1}{p_{22}}(\nabla\sigma + p_{12}\mathbf{u}) \tag{10}$$

obtained from $(4)_2$ into $(4)_1$. From $(4)_1$ and (10) the partial differential equation for the frame displacement vector is

$$\nabla^2\mathbf{u} + A_{31}\nabla\tau + A_{32}\nabla\sigma + B_{33}\mathbf{u} = 0 \tag{11}$$

where

$$A_{31} := \frac{1-\mu a_{11}}{\mu}, \quad A_{32} := a_{12} - \frac{p_{12}}{\mu p_{22}}, \quad B_{33} := \frac{p_{11}p_{22} - p_{12}^2}{\mu p_{22}}.$$

Also note that the third and fourth equations of (6) imply that shear waves in the frame satisfy

$$\nabla^2\varpi + B_{33}\varpi = 0. \tag{12}$$

It is now easy to ascertain the speed of propagation and attenuation of dilatational and shear waves in, for instance, the x-direction. Because the time-harmonic variation has already been incorporated into the coefficients of eqns (9) we seek solutions of the form $\tau(x) = c_1 e^{ik_p x}$ and $\sigma(x) = c_2 e^{ik_p x}$. To represent a physical (spatially decaying) solution the imaginary part of the complex wave number k_p must be positive. Substituting these forms into (9) and requiring the constants c_1 and c_2 to be arbitrary gives the condition

$$(B_{11} - k_p^2)(B_{22} - k_p^2) - B_{12}B_{21} = 0$$

from which two possible physical wave numbers

$$k_{p\pm} = \sqrt{\frac{B_{11} + B_{22} \pm \sqrt{(B_{11} - B_{22})^2 + 4B_{12}B_{21}}}{2}} \tag{13}$$

are obtained. The branch cut for the outer square root is taken to lie along the positive real axis so that $\operatorname{Im} k_{p\pm} \geqslant 0$. The sign of $\operatorname{Re} k_{p\pm}$ may be either positive or negative. If we write $k_{p\pm} = (\omega/c_{p\pm})\,(\operatorname{sgn}(\operatorname{Re} k_{p\pm}) + i\eta\beta_{p\pm})$ where $\eta = \ln 10/(40\pi)$ and the attenuation coefficients $\beta_{p\pm}$ are measured in decibels per wavelength, then the compressional wave speeds and attenuation coefficients for the two waves are given by

$$c_{p\pm} = \frac{\omega}{|\operatorname{Re} k_{p\pm}|}, \quad \beta_{p\pm} = \frac{\operatorname{Im} k_{p\pm}}{\eta|\operatorname{Re} k_{p\pm}|}. \tag{14}$$

A similar analysis of eqn (12) gives

$$k_s = \sqrt{B_{33}},$$

$$c_s = \frac{\omega}{|\mathrm{Re}\, k_s|}, \quad \beta_s = \frac{\mathrm{Im}\, k_s}{\eta |\mathrm{Re}\, k_s|}, \tag{15}$$

for the speed and attenuation of shear waves through the frame.

The compressional waves corresponding to the wave numbers k_{p+} and k_{p-} are sometimes referred to as Type I and Type II compressional waves. Type I compressional waves have speed and attenuation numerically close to those of similar sediments in elastic models of the seabed. Type II compressional waves move much more slowly and are highly attenuated.

For computing transmission loss it is appropriate to work in cylindrical coordinates and suppress the dependence upon the azimuthal variable whence the displacement vectors are now denoted as $\mathbf{u}(r, z) = (u_r(r, z), u_z(r, z))$, $\mathbf{U}(r, z) = (U_r(r, z), U_z(r, z))$. In this situation the constitutive eqns (1) become

$$\sigma_{rr} = \lambda e + 2\mu e_{rr} + Q\varepsilon, \quad \sigma_{zz} = \lambda e + 2\mu e_{zz} + Q\varepsilon,$$
$$\sigma_{rz} = 2\mu e_{rz}, \quad \sigma = Qe + R\varepsilon,$$

and the strain–displacement relations (2) are now

$$e_{rr} = \partial_r u_r, \quad e_{zz} = \partial_z u_z, \quad e_{rz} = \tfrac{1}{2}(\partial_z u_r + \partial_r u_z). \tag{16}$$

In equation (6) the azimuthally independent Laplacian is

$$\nabla^2 := \partial_{rr} + \frac{1}{r}\partial_r + \partial_{zz}.$$

2.2. *Elastic model of a seabed*

In the elastic model of a seabed a layer is treated as a viscoelastic slab depending upon the parameters ρ, the aggregate density of the layer, λ and μ, the compressional and shear Lamé coefficients, and β_p and β_s, compressional and shear attenuation coefficients. In cylindrical coordinates the equations for dilatation $e(r, z)$ and vertical displacement $u_s(r, z)$ in this model (see Kolsky, 1963; Brekhovskikh, 1980, for instance) are

$$(\lambda + 2\mu)\nabla^2 e + \rho\omega^2 e = 0$$
$$\mu\nabla^2 u_z + (\lambda + \mu)\,\partial_z e + \rho\omega^2 u_z = 0. \tag{17}$$

The constitutive equations are

$$\sigma_{rr} = \lambda e + 2\mu e_{rr}, \quad \sigma_{zz} = \lambda e + 2\mu e_{zz}, \quad \sigma_{rz} = 2\mu e_{rz},$$

and the strain–displacement relations are still given by (16).

The speeds of dilatational and shear waves are

$$c_p = \sqrt{\frac{\lambda + 2\mu}{\rho}}, \quad c_s = \sqrt{\frac{\mu}{\rho}}. \tag{18}$$

The experimental inputs for the elastic model are ρ, c_p, c_s, β_p and β_s. Equation (18) and the relations $k_{p,s} = (\omega/c_{p,s})(1 + i\eta\beta_{p,s})$ give equations for the determination of the viscoelastic Lamé coefficients

Table 1. Parameters in the Biot–Stoll model

Symbol	Parameter
ρ_f	Density of the pore fluid
ρ_r	Density of sediment grains
K_b	Complex frame bulk modulus
μ	Complex frame shear modulus
K_f	Fluid bulk modulus
K_r	Grain bulk modulus
β	Porosity
η	Viscosity of pore fluid
k	Permeability
α	Structure factor
a	Pore size parameter

$$\mu = \rho C_s^2, \quad \lambda = \rho(C_p^2 - 2C_s^2)$$

where C_p and C_s are the complex wave speeds defined by

$$C_{p,s} = \frac{\omega}{k_{p,s}} = \frac{c_{p,s}}{1 + i\eta\beta_{p,s}}.$$

2.3. *Determination of the coefficients in the Biot model*

The formulation of the Biot model given in (3) is that used in Biot (1956a). Subsequently the model was recast by Stoll (1974) to depend upon the eleven parameters shown in Table 1. The parameters may be grouped into three categories: pore fluid parameters ρ_f, K_f and η; grain parameters ρ_r and K_r; and frame parameters K_b, μ, β, k, α and a. The Biot parameters λ, R, Q, ρ_{11}, ρ_{12}, ρ_{22}, and b in (3) are calculated from the Biot–Stoll data using the following relations

$$\begin{aligned}
\lambda &= H - 2\mu - 2C\beta + M\beta^2 \\
R &= M\beta^2 \\
Q &= \beta(C - M\beta) \\
\rho_{11} &= (1-\beta)\rho_r - \beta(\rho_f - m\beta) \\
\rho_{12} &= \beta(\rho_f - m\beta) \\
\rho_{22} &= m\beta^2 \\
b &= \frac{F\left(a\sqrt{\omega\rho_f/\eta}\right)\beta^2\eta}{k}
\end{aligned} \tag{19}$$

where

$$\begin{aligned}
D &= K_r(1 + \beta(K_r/K_f - 1)) \\
H &= \frac{(K_r - K_b)^2}{D - K_b} + K_b + 4\mu/3 \\
C &= \frac{K_r(K_r - K_b)}{D - K_b} \\
M &= \frac{K_r^2}{D - K_b}
\end{aligned}$$

Table 2. Grain and frame Biot–Stoll parameters for three sand sediments. All dimensioned parameters are in MKS units

Symbol	Fine sand	Coarse sand	Coarse sand, fine gravel
ρ_r	2670	2710	2680
K_b	$4.8\times10^7+6.7\times10^5 i$	$5.2\times10^7+7.4\times10^5 i$	$5.9\times10^7+8.2\times10^5 i$
μ	$6.7\times10^7+4.3\times10^6 i$	$7.4\times10^7+4.7\times10^6 i$	$8.3\times10^7+5.3\times10^6 i$
K_r	4.0×10^{10}	5.6×10^{10}	4.0×10^{10}
β	0.43	0.38	0.30
k	3.12×10^{-14}	7.5×10^{-11}	2.58×10^{-10}
α	1.25	1.25	1.25
a	1.19×10^{-6}	3.3×10^{-5}	1.19×10^{-4}

$$m = \frac{\alpha\rho_f}{\beta}. \tag{20}$$

The multiplicative factor $F(\zeta)$, which was introduced by Biot (1956b) to correct for the invalidity of the assumption of Poiseuille flow at high frequencies, is given by

$$F(\zeta) = \frac{1}{4}\frac{\zeta T(\zeta)}{1-2T(\zeta)/i\zeta} \tag{21}$$

where T is defined in terms of Kelvin functions

$$T(\zeta) = \frac{\mathrm{ber}'(\zeta)+i\,\mathrm{bei}'(\zeta)}{\mathrm{ber}(\zeta)+i\,\mathrm{bei}(\zeta)}.$$

Table 2 gives estimates for the grain and frame parameters of the Biot–Stoll model for three sand sediments. For each sediment the frame bulk modulus and shear modulus were calculated from formula (17) of Stoll and Bryan (1970) assuming a frame rod velocity of $\sqrt{E_b(1-\beta)\rho_r} = 3.0\times10^2$ m/s and a log decrement of $\delta_E = 0.15$ for longitudinal vibrations and a shear velocity of $\sqrt{\mathrm{Re}(\mu)/(1-\beta)\rho_r} = 2.1\times10^2$ m/s and a log decrement of $\delta_s = 0.2$ for shear vibrations. The remaining grain and frame parameter estimates for the fine sand and coarse sand and fine gravel sediment are taken from Holland and Brunson (1988). They are based on measurements at two Italian sites in the Gulf of La Spezia. The estimates for the coarse and sand sediment are from Beebe *et al.* (1982) for the seabed off Daytona Beach, Florida. Estimates for the pore fluid parameters vary little when the interstitial fluid is seawater. In numerical experiments we shall use the values $\rho_f = 1000$ kg/m^3, $K_f = 2.4\times10^9$ N/m^2, $\eta = 1.01\times10^{-3}$ N-s/m^2.

In the elastic model compressional and shear wave speeds are independent of frequency and the attenuation factors depend linearly on frequency. As noted in Stoll (1974) this is not the case for the Biot model, especially for high permeability sediments. Figures 1, 2 and 3 show plots of the two compressional wave speeds and shear wave speed and their attenuation as functions of frequency for each of the sediments in Table 2. As can be seen only the low permeability fine sand sediment fits the assumptions of the elastic model, that is, it has wave speeds which are approximately constant with respect to frequency and attenuations that are approximately log-linear with slope 1.

3. MODAL REPRESENTATION OF ACOUSTIC PRESSURE IN THE OCEAN

In this section we solve the equations of the Biot and elastic models, present appropriate interface conditions and then derive a representation for pressure in the ocean.

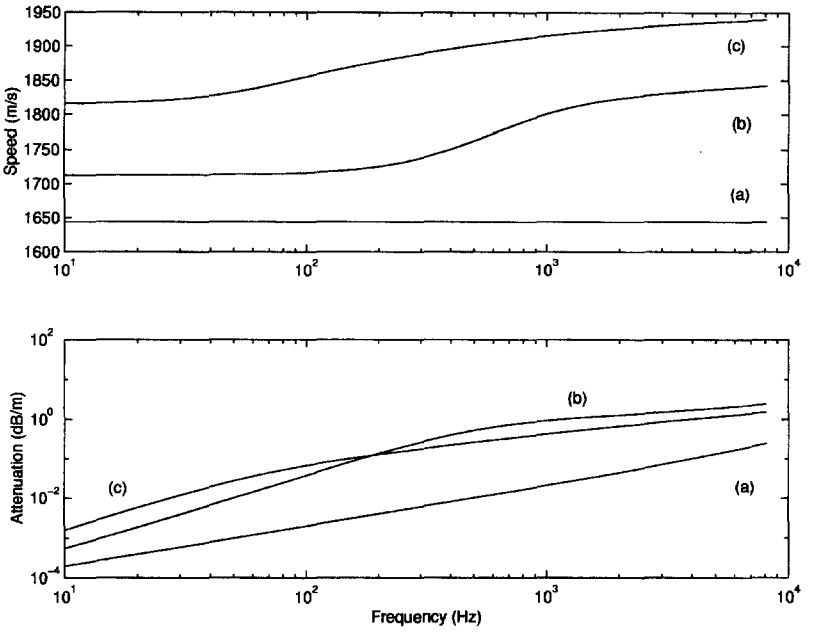

Fig. 1. Biot model's predictions for speed and attenuation for Type I compressional waves as functions of frequency for (a) fine sand; (b) coarse sand; (c) coarse sand, fine gravel.

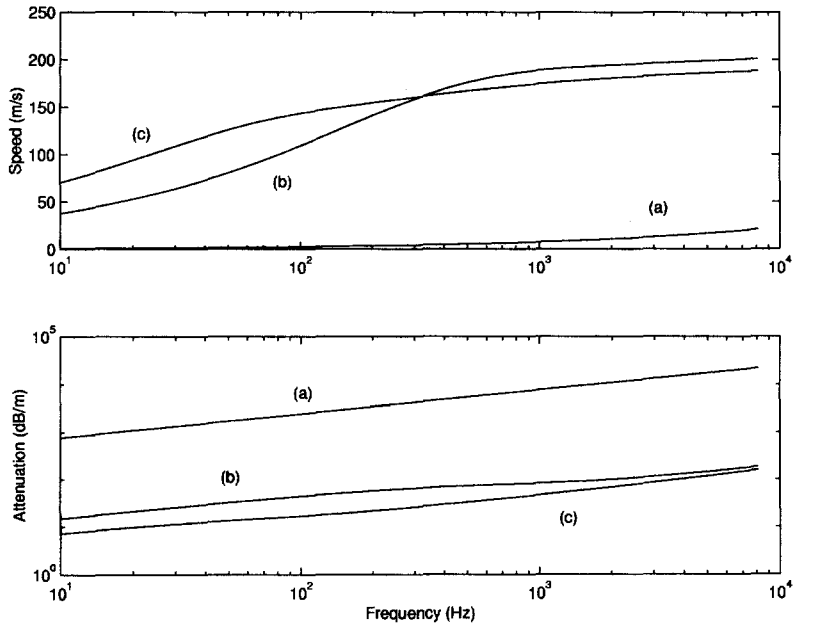

Fig. 2. Biot model's predictions for speed and attenuation of Type II compressional waves as a function of frequency for (a) fine sand; (b) coarse sand; (c) coarse sand, fine gravel.

3.1. *Solution of the differential equations for poroelastic and elastic layers*

We introduce a reference wave number $k_0 = \omega/c_0$, where c_0 is a representative sound speed in the ocean. Solutions of the form

$$\tau(r,z) = \tau(z)H_0^{(1)}\left(k_0\sqrt{\kappa}r\right), \quad \sigma(r,z) = \sigma(z)H_0^{(1)}\left(k_0\sqrt{\kappa}r\right),$$

$$u_z(r,z) = u_z(z)H_0^{(1)}\left(k_0\sqrt{\kappa}r\right), \quad U_z(r,z) = U_z(z)H_0^{(1)}\left(k_0\sqrt{\kappa}r\right),$$

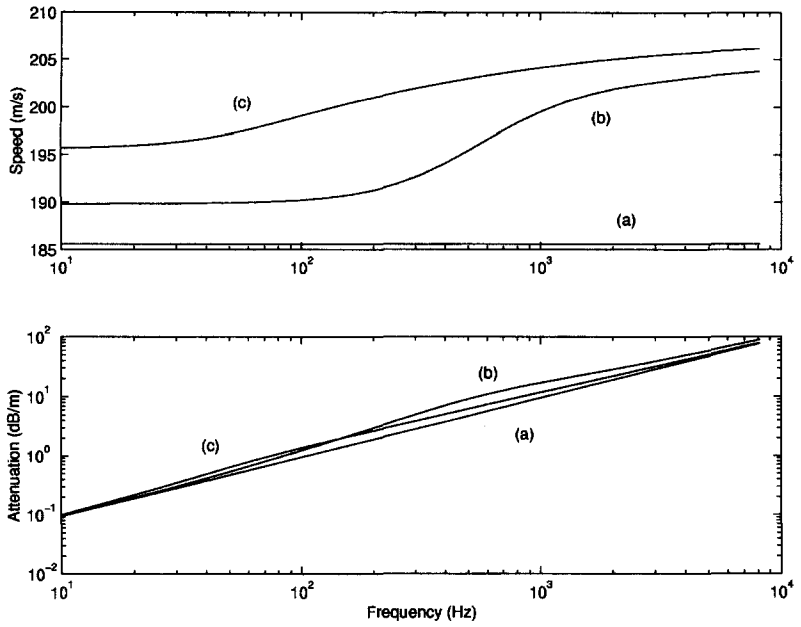

Fig. 3. Biot model's prediction for speed and attenuation of shear waves as a function of frequency for (a) fine sand; (b) coarse sand; (c) coarse sand, fine gravel.

$$u_r(r,z) = u_r(z)H_1^{(1)}\left(k_0\sqrt{\kappa}r\right), \quad U_r(r,z) = U_r(z)H_1^{(1)}\left(k_0\sqrt{\kappa}r\right) \tag{22}$$

are sought where $H_j^{(1)}$, $j = 0, 1$ are outgoing Hankel functions and $\mathrm{Im}(\kappa) \geqslant 0$ is required for solutions to approach zero as $r \to \infty$. Substituting the assumed forms into the system (4) gives

$$\begin{aligned} r''(z) + a_{rs}^2\tau(z) + B_{12}\sigma(z) &= 0 \\ \sigma''(z) + B_{21}\tau(z) + a_{\sigma s}^2\sigma(z) &= 0 \end{aligned} \tag{23}$$

where

$$\begin{aligned} a_{\tau s}^2 &:= B_{11} - k_0^2\kappa = p_{11}a_{11} - p_{12}a_{12} - k_0^2\kappa \\ a_{\sigma s}^2 &:= B_{22} - k_0^2\kappa = p_{22}a_{22} - p_{12}a_{12} - k_0^2\kappa. \end{aligned}$$

The general solutions to this system is

$$\begin{aligned} \tau(z) &= c_1 e^{im_-(z-z_d)} + c_2 e^{-im_+(z-z_d)} + c_3 e^{im_-(z-z_d)} + c_4 e^{-im_-(z-z_d)} \\ \sigma(z) &= \frac{m_+^2}{B_{12}}(c_1 e^{im_-(z-z_d)} + c_2 e^{-im_+(z-z_d)}) + \frac{m_-^2}{B_{12}}(c_3 e^{im_-(z-z_d)} + c_4 e^{-im_-(z-z_d)}) \\ &\quad - \frac{a_{\tau s}^2}{B_{12}}(c_1 e^{im_+(z-z_d)} + c_2 e^{im_+(z-z_d)} + c_3 e^{im_-(z-z_d)} + c_4 e^{-im_-(z-z_d)}) \end{aligned} \tag{24}$$

where z_d is the depth of the layer surface and

$$m_{\pm} := \sqrt{\frac{a_{\tau s}^2 + a_{\sigma s}^2 \pm \sqrt{(a_{\tau s}^2 - a_{\sigma s}^2)^2 + 4B_{12}B_{21}}}{2}}$$

with the branch cut for the square root function is chosen so that $\mathrm{Im}(m_{\pm}) \geqslant 0$. The frame and fluid dilatations now can be computed from (8).

From (11) and (22) the depth factor for vertical displacement of the sediment frame now can be obtained by solving the differential equation

$$u_z''(z) + A_{31}\tau'(z) + A_{32}\sigma'(z) + a_{us}^2 u_z(z) = 0$$

where

$$a_{us}^2 := B_{33} - k_0^2\kappa = \frac{p_{11}}{\mu} - \frac{p_{12}^2}{p_{22}\mu} - k_0^2\kappa.$$

This solution is rather complicated and will not be displayed. It may be found in Buchanan and Gilbert (1996). Note that this solution will depend upon two further arbitrary constants. From (10) vertical displacement of the pore fluid is given by

$$U_z = -\frac{1}{p_{22}}(p_{12}u_z + \partial_z\sigma).$$

Finally the definitions of the dilatations

$$e = \nabla \cdot \mathbf{u} = \partial_r u_r + \frac{1}{r}u_r + \partial_z u_z$$

$$\varepsilon = \nabla \cdot \mathbf{U} = \partial_r U_r + \frac{1}{r}U_r + \partial_z U_z$$

and (22) yield solutions for the depth factors for radial displacement

$$u_r(z) = \frac{1}{k_0\sqrt{\kappa}}(e(z) - u_z'(z))$$

$$U_r(z) = \frac{1}{k_0\sqrt{\kappa}}(\varepsilon(z) - U_z'(z)).$$

Similar solutions can be obtained for the elastic model (17). The dilatation and vertical displacement are

$$e = c_1 e^{ia_s(z-z_d)} + c_2 e^{-ia_s(z-z_d)}$$

$$u_z = iC_s a_s \frac{c_1 e^{ia_s(z-z_d)} - c_2 e^{-ia_s(z-z_d)}}{a_s^2 - b_s^2} + c_3 e^{ib_s(z-z_d)} + c_4 e^{-ib_s(z-z_d)}$$

where

$$a_s^2 := \frac{\rho\omega^2}{\lambda + 2\mu} - k_0^2\kappa, \quad b_s^2 := \frac{\rho\omega^2}{\mu} - k_0^2\kappa, \quad C_s := 1 + \frac{\lambda}{\mu}.$$

3.2. *Interface conditions*

In the ocean acoustic pressure $P_o(r, z)$ and vertical displacement $U_{zo}(r, z)$ arising from a point source located at a depth $z = z_0$ are solutions to the system of differential equations

$$\nabla^2 P_o + k_0^2 P_o = -\frac{1}{2\pi r}\delta(r)\delta(z-z_0)$$

$$\partial_z P_o + \lambda_o k_0^2 U_{zo} = 0$$

where $\lambda_o = \rho_o c_0^2$ is the compressional Lamé coefficient for seawater. We assume the ocean is of constant depth $z = z_d$ and lies over a two-layer seabed. In the upper, sediment, layer we denote the dilatation, vertical displacement and so forth by $e_s(r,z)$, $u_{zs}(r,z),\ldots$, while in the lower, substrate, layer the corresponding quantities are denoted $e_b(r,z)$, $u_{zb}(r,z),\ldots$. The sediment–substrate interface is at a depth $z = z_b$ beneath the ocean surface. At the surface of the ocean a pressure-release condition is imposed

$$P_o(r,0) = 0.$$

The conditions used at the ocean-sediment boundary are specializations of those between sediment layers, hence we treat the interface conditions between layers of each sediment type first. For an interface between two solid elastic layers we require continuity of vertical displacement u_z, normal stress σ_{zz}, tangential stress σ_{rz} and radial displacement u_r. At the boundary $z = z_b$ between the two elastic layers this gives

$$\begin{aligned} u_{zs}(r,z_b-) &= u_{zb}(r,z_b+) \\ \sigma_{zzs}(r,z_b-) &= \sigma_{zzb}(r,z_b+) \\ \sigma_{rzs}(r,z_b-) &= \sigma_{rzb}(r,z_b+) \\ u_{rz}(r,z_b-) &= u_{rb}(r,z_b+). \end{aligned}$$

At the interface $z = z_d$ between the ocean and an elastic sediment the radial displacement condition is dropped and tangential stress is set to zero on the ocean side. This gives

$$\begin{aligned} u_{zo}(r,z_d-) &= u_{zs}(r,z_d+) \\ p_o(r,z_d-) &= \sigma_{zzs}(r,z_d+) \\ \sigma_{rzs}(r,z_d+) &= 0. \end{aligned}$$

At an interface between two poroelastic layers continuity is required for vertical displacement u_z, aggregate normal stress $\sigma_{ss}+\sigma$, pore fluid pressure σ/β, specific flux

$$\beta\frac{\partial}{\partial t}(U_z(r,z,t)-u_z(r,z,t)) = \beta i\omega e^{i\omega t}(U_z(r,z)-u_z(r,z)),$$

tangential stress σ_{rz} and radial displacement u_r. This gives

$$\begin{aligned} u_{zs}(r,z_b-) &= u_{zb}(r,z_b+) \\ \sigma_{zzs}(r,z_b-)+\sigma_s(r,z_b-) &= \sigma_{zzb}(r,z_b+)+\sigma_b(r,z_b+) \\ \sigma_s(r,z_b-)/\beta_s &= \sigma_b(r,z_b+)/\beta_b \\ \beta_s U_{zs}(r,z_b-)+(\beta_b-\beta_s)u_{zs}(r,z_b-) &= \beta_b U_{zb}(r,z_b+) \\ \sigma_{rzs}(r,z_b-) &= \sigma_{rzb}(r,z_b+) \\ u_{rz}(r,z_b-) &= u_{rb}(r,z_b+). \end{aligned} \tag{25}$$

Condition $(25)_4$ was obtained from the continuity of vertical frame displacement and flux conditions. At the interface between the ocean and a poroelastic sediment we use $(25)_4$ with $\beta = 1$ on the ocean side, equate both sediment side normal stress and pore stress to P_o and set tangential stress to zero on the ocean side. This gives

$$U_{zo}(r, z_d-) = \beta_s U_{zs}(r, z_d+) + (1-\beta_s)u_{zs}(r, z_d+)$$
$$P_o(r, z_d-) = \sigma_{zzs}(r, z_d+) + \sigma_s(r, z_d+)$$
$$P_o(r, z_d-) = \sigma_s(r, z_d+)/\beta_s$$
$$\sigma_{rzs}(r, z_d+) = 0. \tag{26}$$

For a poroelastic sediment over an elastic substrate continuity is required for both skeletal and fluid vertical displacement, aggregate normal stress, tangential stress, and radial displacement. This gives

$$u_{zs}(r, z_b-) = U_{zs}(r, z_b-) = u_{zb}(r, z_b+)$$
$$\sigma_{zzs}(r, z_b-) + \sigma_s(r, z_b-) = \sigma_{zzb}(r, z_b+)$$
$$\sigma_{rzs}(r, z_b-) = \sigma_{rzb}(r, z_b+)$$
$$u_{rz}(r, z_b-) = u_{rb}(r, z_b+).$$

In the substrate layer we require as asymptotic conditions that all dilatations and displacements vanish as $z \to \infty$. Thus in the Biot model the solutions (24) have the form

$$\tau(z) = c_1 e^{im_+(z-z_b)} + c_2 e^{im_-(z-z_b)}$$
$$\sigma(z) = \frac{m_+^2}{B_{12}} c_1 e^{im_+(z-z_b)} + \frac{m_-^2}{B_{12}} c_2 e^{im_-(z-z_b)} - \frac{a_{ts}^2}{B_{12}}(c_1 e^{im_+(z-z_b)} + c_2 e^{im_-(z-z_b)})$$

in the substrate layer.

3.3. *Modal representation of far field transmission loss*

We now construct a modal representation for acoustic pressure in the ocean, following the formulation presented in Boyles (1984). The process is similar irrespective of which model, elastic or poroelastic, is used for each sediment layer. We illustrate with the case of a poroelastic sediment over a poroelastic substrate. More detail can be found in Buchanan *et al.* (1997). A Green's function representation

$$P_o(r, z, z_0) = \frac{k_0^2}{8\pi} \oint_{\mathscr{C}_0} H_0^{(1)}(k_0\sqrt{\kappa}r) G_2(z_1, z_0, \kappa)\, d\kappa \tag{27}$$

is sought. The contour $\mathscr{C}_0$ must enclose all singularities of G_2 and exclude those of $H_0^{(1)}(k_0\sqrt{\kappa}r)$. We choose it to be the slit cut enclosing the positive real axis, oriented counterclockwise. The depth Green's function G_2 then satisfies the differential equation

$$\frac{d^2 G_2}{dz^2} + a_o^2 G_2 = -\delta(z-z_0) \tag{28}$$

where $a_o := k_0\sqrt{1-\kappa}$ with the interface conditions

$$G_2(0, z_0, \kappa) = 0 \tag{29}$$

at the ocean surface

$$G_2(z_0-,z_0,\kappa)=G_2(z_0+,z_0,\kappa)\frac{dG_2}{dz}(z_0+,z_0,\kappa)-\frac{dG_2}{dz}(z_0-,z_0,\kappa)=-1 \tag{30}$$

at the source depth. The general solution to (28) which satisfies the interface conditions (29) and (30) is

$$G_2(z,z_0,\kappa)=C_1\sin a_o z-\frac{H(z-z_0)}{a_o}\sin a_o(z-z_0),\quad 0\leqslant z\leqslant h$$

where H is the unit step function.

In the sediment layer the solutions $e_s(z)$, $\varepsilon_s(z)$ and $u_{zs}(z)$ depend upon six arbitrary constants which we now designate as $C_2,\ldots,C_7$. Due to the asymptotic conditions the solution in the substrate layer depends upon only three arbitrary constants C_8, C_9, C_{10}. Employing the ten interface conditions (26) and (25) with $G_2(z,z_0,\kappa)$ replacing P_o and $-(1/k_0^2\lambda_o)(dG_2/dz)\,(h-,z_0,\kappa)$ replacing u_{zo} gives a matrix equation

$$\mathscr{M}\begin{bmatrix}\frac{C_1}{\lambda_o}\\ C_2\\ C_3\\ C_4\\ \vdots\\ C_{10}\end{bmatrix}=\begin{bmatrix}-\frac{1}{k_0^2\lambda_o}\cos a_o(z_d-z_0)\\ \frac{1}{a_o}\sin a_o(z_d-z_0)\\ \frac{1}{a_o}\sin a_o(z_d-z_0)\\ 0\\ \vdots\\ 0\end{bmatrix} \tag{31}$$

for the determination of the arbitrary constants $C_1,\ldots,C_{10}$.

The singularities of G_2 are those of the constant C_1, which from (31) has the representation

$$C_1=\lambda_0\frac{\Delta_1}{\Delta_0}$$

where $\Delta_0:=\det(\mathscr{M})$ and Δ_1 is the numerator determinant for C_1 in Cramer's rule. The singularities are thus the zeros of Δ_0 (the eigenvalues of the problem) and any non-trivial branch cuts. These are the $m_{s\pm}$, a_{us}, $m_{b\pm}$, and a_{ub} branch cuts. See Buchanan *et al.* (1997) for an explanation as to why the other apparent branch cuts are trivial. To compute the contour integral in (27) we introduce counterclockwise slit cuts $\mathscr{C}_{ms_\pm}$, $\mathscr{C}_{mb_\pm}$, $C_{a_{us}}$ and $\mathscr{C}_{a_{ub}}$ about the six branch cuts. The depth Green's function is now analytic outside of the contour $\mathscr{C}_{ms_+}+\mathscr{C}_{ms_-}+\mathscr{C}_{a_{us}}+\mathscr{C}_{mb_+}+\mathscr{C}_{mb_-}+\mathscr{C}_{a_{ub}}$ except at the eigenvalues $\{\kappa_n\}$. Computing the residues at the eigenvalues gives the following representation for pressure

$$P_o(r,z,z_0)=\sum_n\frac{k_0^2\lambda_0 i}{4}\frac{\Delta_1(\kappa_n)}{\frac{d\Delta_0}{d\kappa}(\kappa_n)}\sin(a_o(\kappa_n)z)H_0^{(1)}(k_0\sqrt{\kappa_n}r)$$

$$-\frac{k_0^2}{8\pi}\oint_{\mathscr{C}_{ms_+}-\mathscr{C}_{ms_-}+\mathscr{C}_{a_{us}}+\mathscr{C}_{mb_+}+\mathscr{C}_{mb_-}+\mathscr{C}C_{a_{ub}}}G_2(z,z_0,\kappa)H_0^{(1)}(k_0\sqrt{\kappa}r)\,d\kappa. \tag{32}$$

As indicated in Buchanan *et al.* (1997) the integrals along the branch cuts are significant contributors only near the source, typically out to a distance of less than 1 km, and thus the summation part of (27) suffices for the representation of acoustic pressure in the far

Table 3. Geoacoustical parameters for a Daytona Beach site. All units are MKS

Layer	Depth	Density	Comp. vel.	Shear vel.
Ocean	32	1000	1530	
Sediment	10	2100	1723	
Substrate	∞	2200	2222	670

Table 4. Parameters for the elastic model of three sand sediments. Densities and velocities are in MKS units. Attenuation factors are in dB/wavelength

Parameter	Fine sand	Coarse sand	Coarse sand, fine gravel	Substrate
ρ	1950	2060	2176	2200
c_p	1647	1723	1847	2222
β_p	0.032	0.53	1.21	0.25
c_s	186	190	198	670
β_s	1.75	2.22	2.67	1.0

field. In the representation (32) the eigenvalues $\{\kappa_n\}$ are found numerically by minimizing $|\Delta_0(\kappa)|$. This has been found more reliable than solving $\Delta_0(\kappa) = 0$ numerically. The derivatives $(d\Delta_0/d\kappa)(\kappa_n)$ are also computed numerically. In the numerical trials presented in the next section we will be concerned with transmission loss as a function of frequency. Transmission loss, normalized to be zero one meter from a point source, is

$$TL = -20\log(4\pi|P_o(r, z, z_0)|). \tag{33}$$

4. PREDICTIONS OF THE ELASTIC AND POROELASTIC MODELS FOR A ONE-LAYER SEABED

In the numerical experiments that follow we shall use the geoacoustical parameters for a Daytona Beach site given in Beebe *et al.* (1982). These are shown in Table 3. The ocean was determined to have approximately constant sound speed and the depth was independent of range. For the short range experiments described in Beebe *et al.* (1982) the source depth was 18 m and the receiver depth was 16 m.

The Biot–Stoll parameters of Table 2 will be used for the poroelastic model. Table 4 shows the corresponding parameters for the elastic model. For the three sand sediments the densities in the elastic case were computed from the formula

$$\rho = (1-\beta)\rho r + \beta\rho_f. \tag{34}$$

For coarse sand the measurement of Table 3 was used for compressional wave speed c_p. For the other two sands formula (14) with a frequency of 80 Hz was used to calculate compressional wave speed. For all three sands compressional attenuation and shear speed and attenuation were computed from formulas (14) and (15), again at a frequency of 80 Hz. For the substrate, characterized in Beebe *et al.* (1982) as semi-consolidated, attenuation parameters were not measured. The attenuation parameters used in Table 4 were those given in Hughes *et al.* (1990) for a chalk sediment having similar compressional and shear velocities.

We first compare the predictions of the Biot model with the elastic model over a one-layer seabed. Such a model would be expected to be accurate for frequencies sufficiently high that the surficial layer of sediment is dominant in determining the transmission loss. The geoacoustical parameters used were those of Table 3, but the sediment layer was

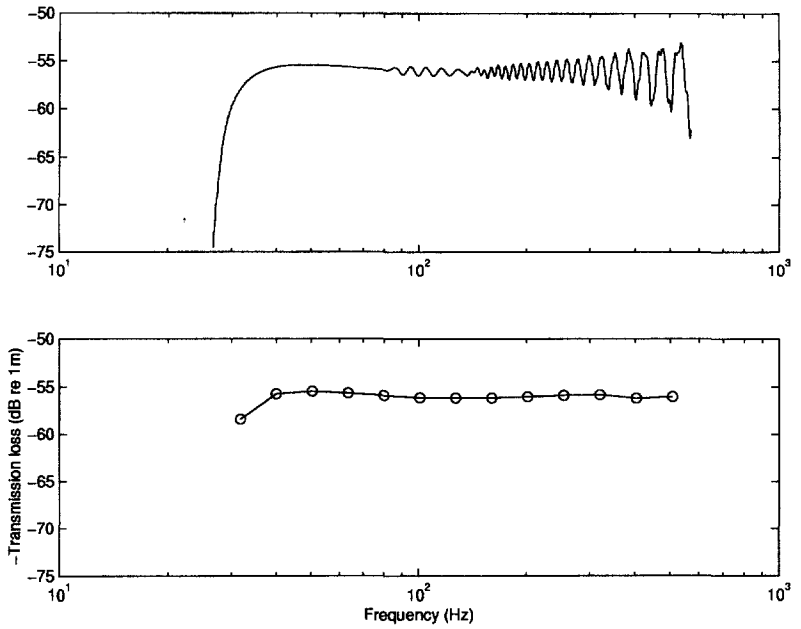

Fig. 4. Top: Transmission loss as a function of frequency for coarse sand at a range of 3.5 km. Bottom: Transmission loss averaged over one-third octave intervals.

taken to be semi-infinite and hence the substrate layer was ignored. Fig. 4 (Top) shows transmission loss as a function of frequency at a range of 3.5 km for the coarse sand sediment with the Biot–Stoll parameters given in Table 2. As frequency increases more modes in the representation (32) propagate strongly to the far field and transmission loss becomes more oscillatory. Hence in order to compare the loss predictions of different models more easily we shall work with loss averages computed over one-third octave intervals. These are obtained by averaging the modulus of $P_o(r, z, z_0)$ at intervals of less than 1 Hz over a one-third octave interval and using this average in lieu of P_o in (33). The result of this averaging procedure is shown in Fig. 4 (Bottom).

Figure 5 compares the predictions at two source-receiver ranges of halfspace Biot model for the three sand sediments of Table 2 with those of the halfspace elastic model using the estimates in Table 4. As expected in the case of the low permeability fine sand sediment which, as noted earlier, fits the assumptions of the elastic model well, the two models make the same predictions. This is not the case for the two coarser sediments where the Biot model predicts losses up to 10 dB greater in the middle range of frequency at the longer of the two source receiver ranges.

5. PREDICTIONS OF THE ELASTIC AND POROELASTIC MODELS FOR A TWO-LAYER SEABED

Figure 6 shows predictions for transmission loss for the coarse sand sediment of Table 2 at ranges of 3.5 and 11.2 km for two models of the seabed, one consisting of an elastic sediment over an elastic substrate (elastic–elastic model) and the other of a poroelastic sediment over an elastic substrate (poroelastic–elastic model). In the 200–600 Hz range the discrepancy between the results of the two models is about the same as that of the halfspace models (Fig. 5), however the two models are also in substantial disagreement in the one-third octave intervals from 50–80 Hz. Moreover in this frequency range the experimental data in Beebe *et al.* (1982), Fig. 6, is in better agreement with the predictions of the elastic–elastic model. The sharp resonances forecast by the poroelastic–elastic model in the 50–80 Hz range were not observed.

The difficulty with the poroelastic–elastic model derives from the behavior of its eigenvalues. Figure 7 (Top) shows the eigenvalues maps for the elastic and poroelastic

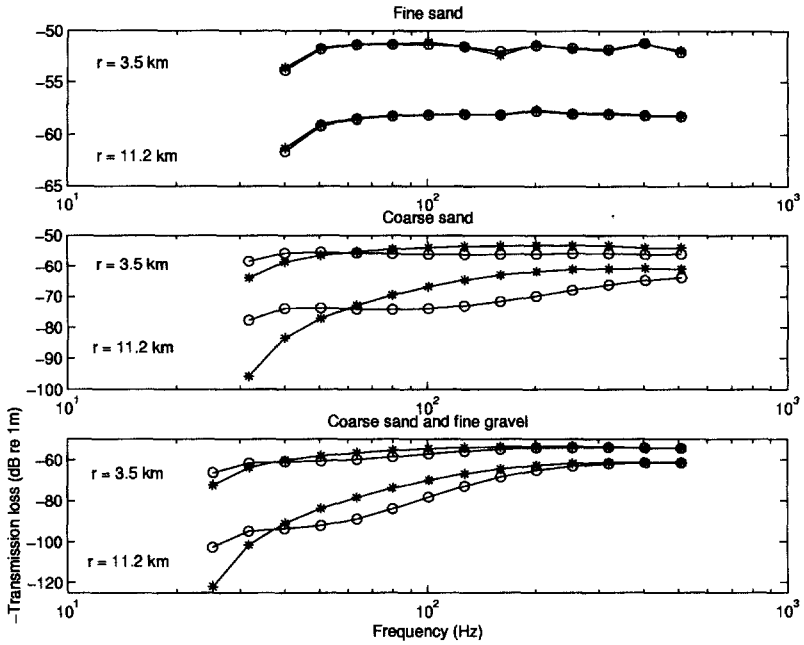

Fig. 5. Comparison of transmission loss for three sediments as predicted by the halfspace Biot model (○) and the halfspace elastic model (*). The source depth was 18 m and the receiver depth 16 m.

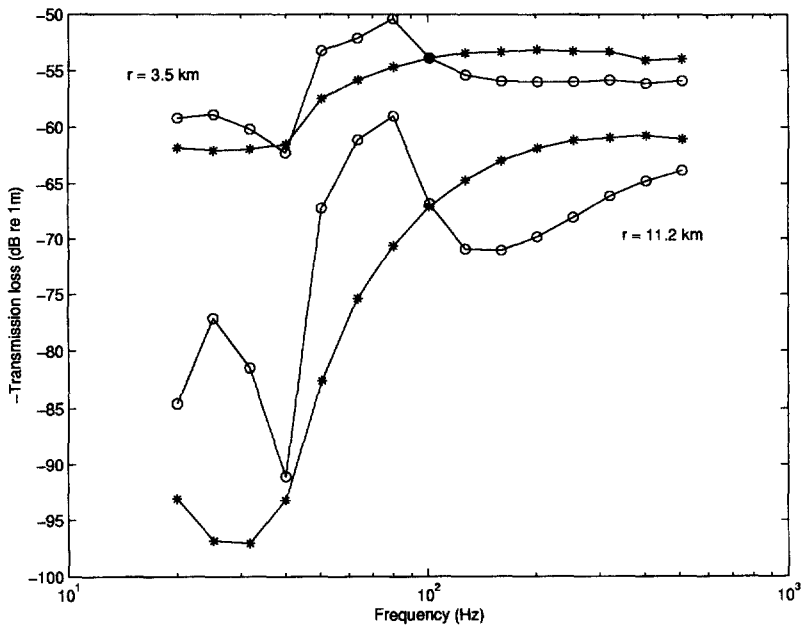

Fig. 6. Transmission loss for coarse sand as predicted for (*) an elastic sediment over an elastic substrate, (○) a poroelastic sediment over an elastic substrate.

halfspace models at 571 Hz. Only eigenvalues lying near the real-axis between $\kappa = 0$ and $\kappa = 1$ make significant contributions to far-field acoustic pressure. Both eigenvalue maps exhibit the "leaky mode" phenomenon common in underwater acoustical models, that is, eigenvalues emerge from branch cuts at certain frequencies. While, as indicated above, there are three non-trivial branch cuts in a poroelastic layer and two in an elastic layer, only one in each case, the a-branch cut for an elastic sediment or the m_+-branch cut for poroelastic layers, lies near the interval $0 \leqslant \kappa \leqslant 1$. The m_+-branch cut runs horizontally leftward from the point

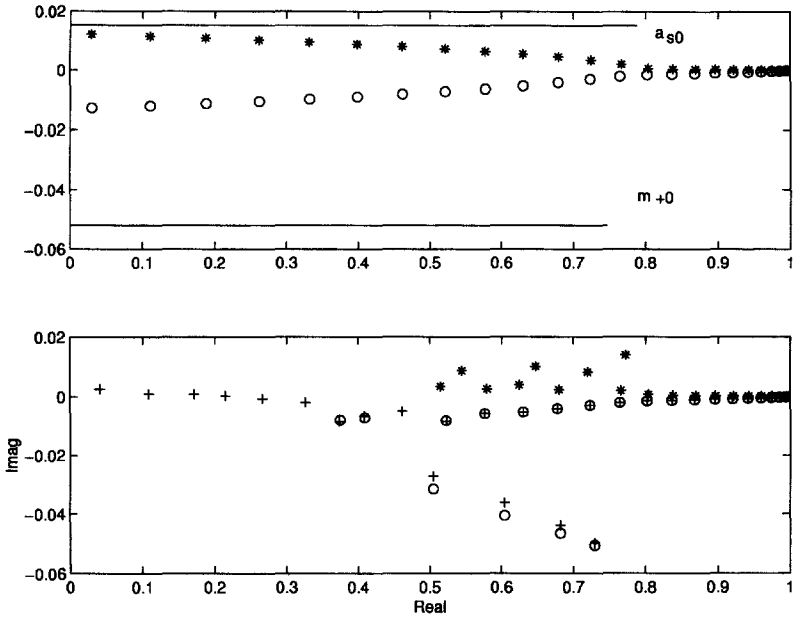

Fig. 7. Top: Eigenvalue maps at 571 Hz for a coarse and halfspace sediment. Eigenvalues for the elastic model (*) emerge from the a_s-branch cut and migrate toward $\kappa = 1$. Those for the poroelastic model from the m_+-branch cut. Bottom: Eigenvalues for a coarse sand sediment over a semi-consolidated substrate for the elastic–elastic model (*); for the poroelastic–elastic model (+); for the poroelastic–elastic model (○).

Table 5. Branch cut locations for three poroelastic sediments and the corresponding elastic models at 80 Hz

	Fine sand	Coarse sand	Coarse sand, fine gravel
m_{+0}	$0.866-0.001i$	$0.796-0.015i$	$0.686-0.303i$
a_0	$0.863+0.001i$	$0.788+0.015i$	$0.686+0.030i$

$$m_{+0} = \frac{B_{11}+B_{22}+\sqrt{(B_{11}-B_{22})^2+4B_{12}B_{21}}}{2k_0^2}$$

and the a-branch cut runs horizontally leftward from the point

$$a_0 = \frac{\rho c_0^2}{\lambda+2\mu}.$$

Table 5 shows the location at 80 Hz of the m_+-branch cuts for the three poroelastic parameter sets of Table 2 and the a-branch cut for the corresponding elastic models of Table 4. As can be seen in Fig. 7 (Top) eigenvalues for halfspace models emerge from the relevant branch cut and migrate toward $\kappa = 1$ as frequency increases. Empirically, the eigenvalues are observed to stay on the same side of the real axis, the positive side in the elastic case, the negative side in the poroelastic case as the branch cut that emitted them.

Figure 7 (Bottom) shows eigenvalue maps for the two-layer seabed consisting of coarse sand over the semi-consolidated substrate of Table 4 for the elastic–elastic, poroelastic–elastic and poroelastic–poroelastic models. For the poroelastic version of the substrate the parameter set Uncons, which will be discussed later was used. In two-layer seabeds eigenvalues seem to emerge from the substrate branch cut, at least in the range of frequencies, 20–600 Hz considered in this article. When the elastic model is used for the upper, sediment, layer eigenvalues emerging from the a_b-branch cut stay on the positive side of the real axis,

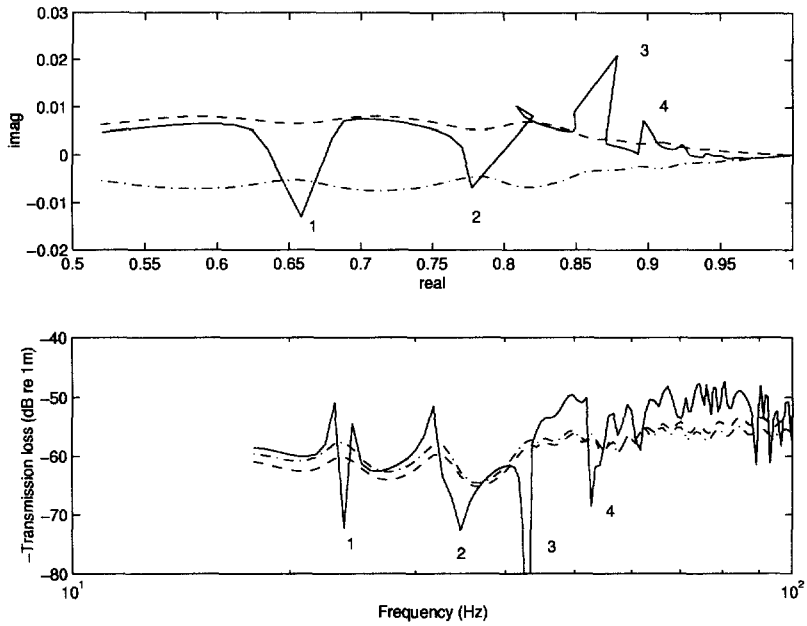

Fig. 8. Top: Paths of the first-detected eigenvalue for a coarse sand sediment over a semi-consolidated substrate for the elastic–elastic model (dashed line); the poroelastic–elastic model (solid line); the poroelastic–elastic model (dash–dotted line). Bottom: Transmission loss as a function of frequency for each model. The effects of the peregrinations of the eigenvalue for the poroelastic–elastic model on transmission loss are indicated by 1–4. The consistent discrepancies between the poroelastic–elastic and the other two models in the frequency range 50–100 Hz are due in part to subsequent eigenvalues.

though their approach to $\kappa = 1$ is not monotonic as in the halfspace case. For the parameters used here the tip of the a_b-branch cut is at $0.474 + 0.004i$. Similarly when poroelastic models are used for both the sediment and substrate, eigenvalues stay below the real axis. When a poroelastic model is used for the sediment layer and an elastic model for the substrate layer, however, eigenvalues emerge from the a_b-branch cut and then cross the real axis. Eigenvalues very near the real axis propagate strongly to the far field and the crossings of the first few eigenvalues are the source of the resonance between 50 and 80 Hz that is seen in Fig. 6. As eigenvalues would be expected to assume their halfspace configuration at high frequencies, which in the case of a poroelastic sediment would put them below the real axis, these resonances seem to be inevitable in a poroelastic–elastic model, and as indicated previously, they are not in accord with observation. Thus, models consisting of poroelastic sediments over elastic substrates appear to be mathematically incompatible.

Another indication that the poroelastic–elastic model is problematic is given by Fig. 8 (Top), which traces the path of the first-detected eigenvalue with increasing frequency for each of the three cases. Whereas this eigenvalue follows paths which regularly approach and digress from the real axis and are approximately symmetric about it in the elastic–elastic and poroelastic–poroelastic case, its motion is much more irregular in the poroelastic–elastic case. As would be expected its course at low frequencies is close to that of the elastic–elastic case and close to that of the poroelastic–poroelastic case at high frequencies. Less expected is its peripatetic behavior at intermediate frequencies which results in the series of resonance-null sequences shown in Fig. 8 (Bottom).

The failure of the poroelastic–elastic model to produce reasonable predictions is unfortunate as it is difficult to estimate even the five parameters in the elastic model for the substrate and much more so for the thirteen parameters of the Biot–Stoll model. Here is the approach we shall take in obtaining a set of poroelastic parameters for a substrate. It will be assumed that a set of elastic parameters for the substrate has been determined. If the substrate layer is a consolidated or semi-consolidated version of the sediment layer,

Table 6. Two Biot–Stoll parameter sets for the substrate

Symbol	Cons	Uncons
ρ_r	2710	2710
K_b	$3.0\times10^9+6.7\times10^7 i$	$3.0\times10^9+6.5\times10^7 i$
μ	$9.9\times10^8+3.6\times10^7 i$	$9.9\times10^8+3.3\times10^7 i$
K_r	5.6×10^{10}	5.6×10^{10}
β	0.30	0.30
k	2.0×10^{-12}	2.8×10^{-11}
α	1.25	1.25
a	5.3×10^{-6}	2.5×10^{-5}
m_{b+0}	$0.473-0.0043i$	$0.473-0.0043i$

then it seems reasonable to use the same grain and fluid parameters for the substrate. Porosity is then inferred from ρ, ρ_r and ρ_f via formula (34). For the substrate with elastic parameters in Table 4 this gives a porosity of about $\beta = 0.30$. Estimating permeability is problematic. The techniques for calculating permeability used in Beebe *et al.* (1982) and Holland and Brunson (1988) require statistics on the grain size distribution which are found from core or grab samples. Such statistics will rarely be available for layers below the surficial one. For the elastic substrate of Table 4 we shall generate estimates for the permeability using two starting points. First we start with the estimate $\beta_1 = 0.28$, $k_1 = 1.5\times10^{-8}$ cm^2 for high porosity sandstone taken from Collins (1961), Figs 1–7. These estimates are then used in the Kozeny–Carmen formula (Holland and Brunson, 1988)

$$k = \frac{\beta^3}{5S_0^2(1-\beta)^2} \tag{35}$$

to determine a value for the specific surface area S_0. The value of S_0 and the target porosity are then used in (35) to obtain an estimate of permeability. This approximation is crude since S_0 is also expected to change with the degree of consolidation. Following Stoll (1974) the pore size parameter is taken to be

$$a = \frac{\sqrt{k}}{0.26}. \tag{36}$$

As the second starting point we use the porosity and permeability of the unconsolidated upper layer, $\beta_1 = 0.38$, $k_1 = 7.5\times10^{-7}$ cm^2 and apply the same estimation process. Having thus obtained estimates for β and k, the values of $\mathrm{Re}\,K_b$, the log decrements δ_b and δ_s and the Poisson ratio R_p are manipulated in the formulas

$$\mathrm{Re}\,K_b = \frac{2}{3}\frac{1+R_p}{1-2R_p}\mathrm{Re}\,\mu, \quad \mathrm{Im}\,K_b = \frac{\delta_b}{\pi}\mathrm{Re}\,K_b, \quad \mathrm{Im}\,\mu = \frac{\delta_s}{\pi}\mathrm{Re}\,\mu \tag{37}$$

so that eqns (14) and (15) give values for the Type I compressional and shear speeds and attenuations that match the target elastic configuration. All parameters other than β, k, a, K_b and μ are simply transferred from the upper layer. We shall refer to the substrate with the permeability of sandstone as a starting point as Cons and the one starting with the permeability of the unconsolidated layer as Uncons. Table 6 shows the two parameter sets for the substrate. Observe that the permeability in these two parameter sets differs by an order of magnitude with a corresponding difference in the pore size parameter, but that all other parameters are about the same. Thus, since the pore size parameter is of negligible consequence at low frequencies, effectively, the significance of the permeability of the substrate is being tested.

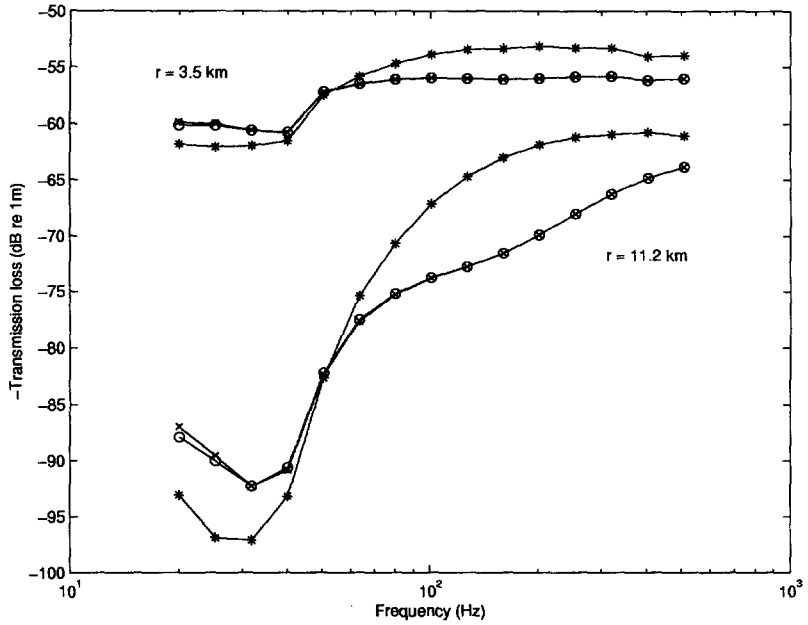

Fig. 9. Comparison of three models of a two-layer sediment for the (*) elastic model for coarse sand over an elastic semi-consolidated substrate; (×) poroelastic model for coarse sand over the poroelastic substrate Cons; (○) poroelastic model for coarse sand over the poroelastic substrate Uncons.

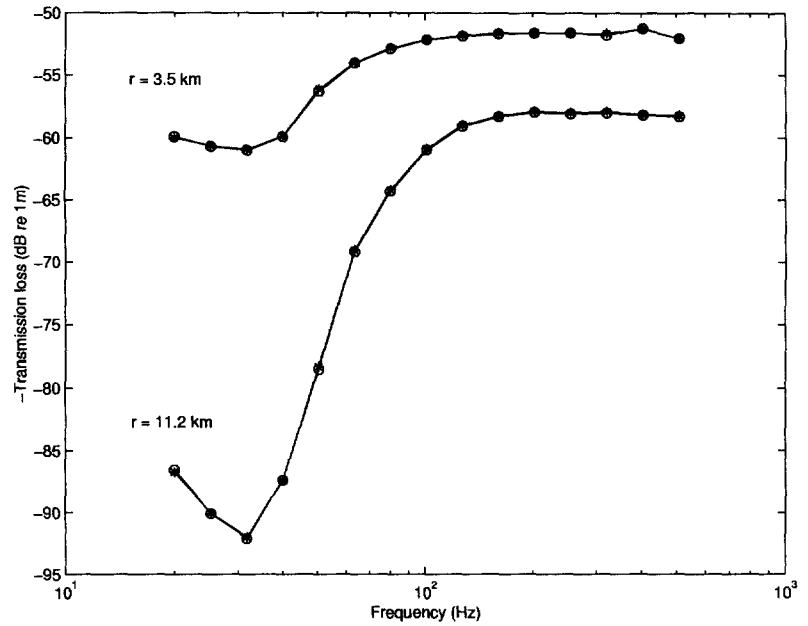

Fig. 10. Comparison of two models of a two-layer sediment for the (*) elastic model for fine sand over an elastic semi-consolidated substrate; (○) poroelastic model for fine sand over the poroelastic substrate Uncons.

Figure 9 shows transmission loss curves for the coarse and sediment of Table 2 over both of the substrates in Table 6. The difference in the permeability of the two substrates had little effect on the predictions. At a source-receiver range of 11.2 km both cases predicted about 5–10 dB less loss at low frequencies than the elastic–elastic model of the same two-layer sediment. At high frequencies the discrepancies between the poroelastic and elastic models were the same as predicted by the respective halfspace models. Figures 10 and 11

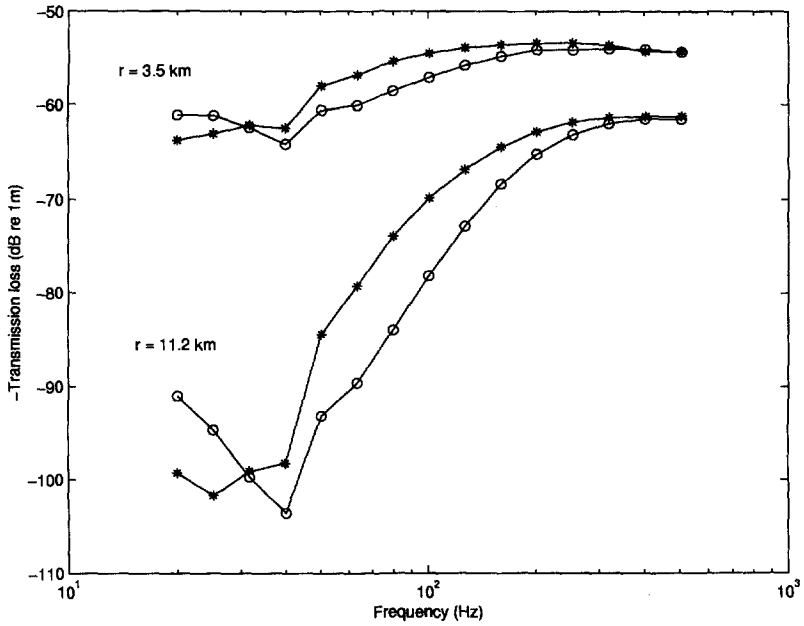

Fig. 11. Comparison of two models of a two-layer sediment for the (*) elastic model for coarse sand and fine gravel over an elastic semi-consolidated substrate; (O) poroelastic model for coarse sand and fine gravel over the poroelastic substrate Uncons.

compare the predictions of the elastic–elastic model and the poroelastic–poroelastic model when the surficial sediments are fine sand and coarse sand and fine graved, respectively, both over the substrate Uncons. The predictions for the coarse and fine gravel sediment were similar to those for the coarse sand sediment. At the longer range, 11.2 km, losses were up to about 10 dB less at low frequencies and up to 10 dB higher in the middle range of frequencies. In the case of the fine sand sediment for which the prediction of the elastic and poroelastic halfspace models were virtually identical, adding a substrate did not change the coincidence of the predictions of the two models, even though the porosity of the substrate was not insignificant. This suggests that the factors specific to a porous medium are of secondary importance in layers below the surficial one and thus crude estimations of these parameters such as were used above may suffice. Figure 12 shows the predictions of the two models when the sediment depth is decreased to 5 and then 2.5 m. The predictions remain within 2 dB of each other, indicating that precise estimation of the poroelastic parameters of the substrate layer may be necessary only when the surficial layer is very thin.

6. CONCLUSION

The elastic and Biot models appear to be mathematically incompatible. One model or the other should be used for all sediment layers. This conclusion is predicated on three empirical observations: (1) eigenvalues emerge from the substrate branch cuts, at least at low frequencies; (2) for parameter sets derived from actual sediments the branch cut relevant to far-field propagation lies above the real axis for the elastic model, but below it for the poroelastic model; (3) the eigenvalues dominating the far-field propagation assume the configuration of those of the halfspace model of the surficial sediment, which puts them below the real axis when the poroelastic model is used. All three observations are in accord with the geoacoustical and sediment parameters used in this article and all others that we have tested, even when the substrate is a low porosity, low permeability sediment such as granite. The three assumptions suffice to cause eigenvalues to cross the real axis which in turn produces frequency intervals in which loss is much lower than is predicted by either

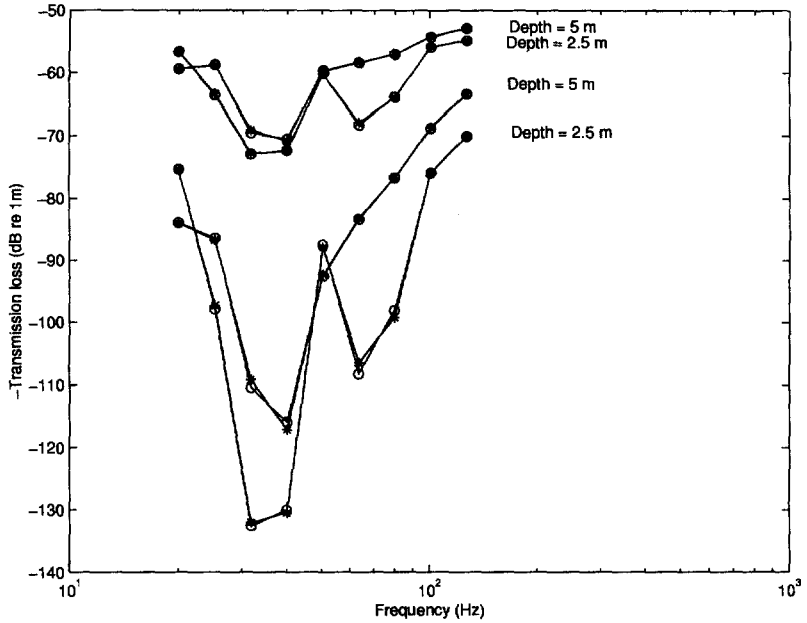

Fig. 12. Predictions of the (*) elastic–elastic model and (○) poroelastic–poroelastic model for surficial sediment depths of 2.5 and 5 m. The upper set of curves is for a source receiver distance of 3.5 km, the lower for 11.2 km.

the elastic–elastic model or the poroelastic–poroelastic model or has been observed in field studies.

Parameter estimation for poroelastic layers below the surficial one poses difficulties, however, it may not be the case that most of the parameters of Biot–Stoll model need to be measured with much precision, unless the suficial layer is very thin. Determination of which poroelastic parameters are important in the lower layers of a seabed awaits further numerical experimentation.

Let us also note that parabolic approximation, an alternative to modal solution for computing acoustic pressure in the far field which is especially useful when complicated range dependencies are present, will be numerically stable for the elastic–elastic and poroelastic–poroelastic cases, but not the poroelastic–elastic case, at least at most frequencies. As discussed in Buchanan and Gilbert (1998) the algorithm can be made stable if it is known *a priori* that all eigenvalues lie either above or below the real axis. There is no way known to accommodate the situation in which eigenvalues lie on both sides of the real axis.

The calculations of transmission loss presented in this work are in accord with the finding of Stoll (1974, 1977) and others that the elastic and Biot model's predictions will differ most for coarse, high permeability sediments.

Acknowledgements—This research was supported in part by the National Science Foundation through Grant BES-9402539.

REFERENCES

Beebe, J., McDaniel, S. and Rubano, L. (1982) Shallow-water transmission loss prediction using the Biot sediment model. *Journal of the Acoustic Society of America* **71**(6), 1417–1426.

Biot, M. (1956a) Theory of propagation of elastic waves in a fluid-saturated porous solid. I. Lower frequency range. *Journal of the Acoustic Society of America* **28**(2), 168–178.

Biot, M. (1956b) Theory of propagation of elastic waves in a fluid-saturated porous solid. II. Higher frequency range. *Journal of the Acoustic Society of America* **28**(2), 179–191.

Biot, M. (1962) Mechanics of deformation and acoustic propagation in porous media. *Journal of Applied Physics* **33**, 1482–1498.

Boyles, C. (1984) *Acoustic Waveguides*. John Wiley and Sons, New York.

Brekhovskikh, L. (1980) Waves in layered media, Vol. 16. *Applied Mechanics and Mechanics*, 2nd edn. Academic Press, New York.

Brunson, B. and Johnson, R. (1980) Laboratory measurements of shear wave attenuation in saturated sand. *Journal of the Acoustic Society of America*. **68**(5), 1371–1375.

Buchanan, J. and Gilbert, R. (1996) Transmission loss in the far field over a seabed with rigid substrate assuming the Biot sediment model. *Journal of Computational Acoustics* **4**(1), 29–54.

Buchanan, J. and Gilbert, R. (1997) Transmission loss in the far field over a one-layer seabed assuming the Biot sediment model. *ZAMM* **77**(2), 121–135.

Buchanan, J. and Gilbert, R. (1998) Comparison of the solution to a problem in ocean acoustics by parabolic approximation with the exact solution obtained from the residue calculus, submitted.

Buchanan, J., Gilbert, R. and Xu, Y. (1997) Green's function representation for acoustic pressure over a poroelastic seabed. *Applicable Analysis* **65,** 57–68.

Collins, R. (1961) *Flow of Fluids through Porous Materials*. Reinhold, New York.

Holland, C. and Brunson, B. (1988). The Biot–Stoll sediment model: an experimental assessment. *Journal of the Acoustic Society of America* **84**(4), 1437–1443.

Hughes, S., Ellis, D., Chapman, D. and Stahl, P. (1990) Low-frequency acoustic propagation loss in shallow water over hard-rock seabeds covered by a thin layer of elastic–solid sediment. *Journal of the Acoustic Society of America* **88**(1), 283–297.

Ingenito, F., Ferris, R., Kuperman, W. and Wolf, S. (1978) Shallow water acoustics: summary report (first phase), Technical Report 8179, Naval Research Laboratory.

Kolsky, H. (1963) *Stress Waves in Solids*. Dover, New York.

Stoll, R. (1974) Acoustic waves in saturated sediments. In *Physics of Sound in Marine Sediments*, ed. L. Hampton, pp. 19–39. Plenum, New York.

Stoll, R. (1977) Acoustic waves in ocean sediments. *Geophysics* **42**(4), 715–725.

Stoll, R. and Bryan, G. (1970) Wave attenuation in saturated sediments. *Journal of the Acoustic Society of America* **47**(5 (Part 2)), 1440–1447.

Vidmar, P. (1980a) The effect of sediment rigidity on bottom reflection loss in a typical deep sea sediment. *Journal of the Acoustic Society of America* **68,** 634–638.

Vidmar, P. (1980b) Ray path analysis of sediment shear wave effects on bottom reflection loss. *Journal of the Acoustic Society of America* **68,** 639–648.

Yamamoto, T. (1983a) Acoustic propagation in the ocean with a poro-elastic bottom. *Journal of the Acoustic Society of America* **73,** 1587–1596.

Yamamoto, T. (1983b) Propagator matrix for continuously layered porous seabeds. *Bull. Seism. Soc. Am.* **73,** 1599–1620.